Journal of Microscopy, Vol. 205, Pt 1 January 2002, pp. 86–95
Received 11 April 2001; accepted 25 July 2001

On the role of electron–ion recombination in low vacuum scanning electron microscopy

M. TOTH, B. L. THIEL & A. M. DONALD
Polymers and Colloids Group, Cavendish Laboratory, University of Cambridge, Madingley Road, Cambridge, CB3 0HE, U.K.

Key words. Contrast mechanisms, electron–ion recombination, ESEM, low vacuum secondary electron imaging, SEM.

Summary

Here we demonstrate the effects of electron–ion recombination on imaging signals utilized in low vacuum scanning electron microscopes (SEMs). The presented results show that, under normal operating conditions, recombination of ionized gas molecules with secondary electrons (SEs) suppresses a significant fraction of emitted electrons. If the ion flux (and hence the spatial dependence of the SE–ion recombination rate) is laterally inhomogeneous across the imaged region of a specimen, contrast in SE images can be influenced and in some cases (under conditions of high detector field strength and long ionic mean free path) dominated by variations in the recombination rate. Consequently, SE images of features such as topographic asperities can exhibit edge-darkening, leading to inversion of some topographic contrast. Recognition of the extent and nature of electron–ion recombination is required for a correct understanding of processes occurring in variable pressure SEMs and, subsequently, for models of image formation.

Introduction

The use of pressure limiting apertures and differential pumping systems has allowed the realization of scanning electron microscopes (SEMs) that can tolerate specimen chamber pressures in the range 1–20 Torr (0.13–2.7 kPa) while maintaining the electron gun and column at high vacuum ($< 10^{-6}$ Torr, 0.13 mPa) (Danilatos, 1988). The presence of a gas in the specimen chamber allows for imaging of uncoated insulators at high beam energies (Robinson, 1975a; Moncrieff *et al.*, 1978; Danilatos, 1988; Farley & Shah, 1991) and, in instruments that can tolerate chamber pressures in excess of approximately 4 Torr (0.5 kPa), wet and liquid samples (Robinson, 1975b, 1978; Danilatos, 1988; Stokes *et al.*, 1998). However, the conventional Everhart–Thornley secondary electron (SE) detector cannot operate in gaseous environments because of the high voltage (~10 kV) required for efficient scintillation and because of the short mean free path of SEs in the gas (Danilatos, 1990; Mohan *et al.*, 1998). The SE signal can be preserved and amplified by placing a positively biased electrode (usually in the form of a ring located above the specimen, centred on the optical axis of the microscope as shown in Fig. 1) in the specimen chamber (Danilatos, 1990; Farley & Shah, 1991). The electrode bias (V) is typically in the range + 50 to + 600 V. The specimen is placed on a grounded metallic stage that also acts as an electrode in the gas. Emitted SEs are accelerated towards the ring by an electric field generated

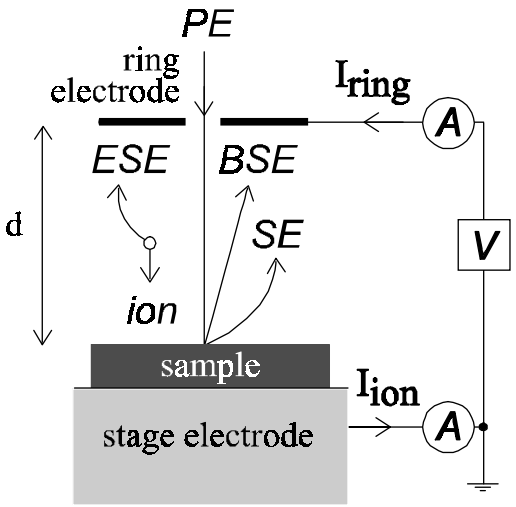

Fig. 1. Schematic illustration of the specimen-biased ring electrode geometry generally employed in variable pressure SEMs. Also shown are the directions in which primary electrons (PEs), backscattered electrons (BSEs), secondary electrons (SEs), environmental secondary electrons (electrons produced in the gas cascade, ESEs) and positive gas ions flow through the gas, the specimen stage (which also acts as an electrode), and current flow induced in the ring and stage electrodes (I_{ring} and I_{ion}, respectively) by the motion of charge carriers in the gas.

Correspondence: M. Toth. Tel.: +44 (0)1223 33 7263; fax: +44 (0)1223 337000; e-mail: mt272@phy.cam.ac.uk

by V. SEs that attain sufficient energy to ionize gas molecules give rise to a gas cascade that can amplify the SE signal by up to three orders of magnitude (Moncrieff *et al.*, 1978; Danilatos, 1990; Meredith *et al.*, 1996; Thiel *et al.*, 1997). The motion of charge carriers between the sample and the ring induces charge flow in the electrodes (ring and specimen stage) (Danilatos, 1990; Farley & Shah, 1991; Durkin & Shah, 1993; Mohan *et al.*, 1998; Toth & Phillips, 2000b). The current induced in the ring is used as the imaging signal in the so-called 'environmental secondary detector' (ESD) (Danilatos, 1990) and the 'gaseous secondary electron detector' (GSED) (FEI, 2000). Alternatively, current induced in the stage (and in the case of a conductive specimen, in the sample), generally termed 'ion current', can also be used as an imaging signal (Farley & Shah, 1990, 1991; Durkin & Shah, 1993; Mohan *et al.*, 1998). As all electron signals between the sample and the ring are amplified in the gas, attainment of images dominated by SE contrast requires appropriate choice of operating parameters such as gas type, gas pressure (P), sample–detector separation (d) and V (Thiel *et al.*, 1997; Fletcher *et al.*, 1997).

Positive ions generated in the cascade drift away from the ring electrode, towards the specimen and the stage (see Fig. 1). During contact with the sample, ions can recombine with electrons in the sample, or with emitted electrons (Hagstrum, 1978; Varga & Winter, 1992; Hahn, 1997; Toth *et al.*, 2000). In general, the efficiency with which ions recombine with emitted (free) electrons decreases with increasing electron energy (von Engel, 1965; Nasser, 1971; Hahn, 1997). Based on experimental and theoretical data in the literature (Hahn, 1997), the SE–ion recombination rate is expected to be at least a few orders of magnitude greater than the rate at which ions recombine with primary and backscattered electrons (BSEs) under all conditions attainable in low vacuum SEMs. The rate at which ions recombine with electrons at the sample surface depends on the electronic properties of the surface and of the ion (Hagstrum, 1978; Varga & Winter, 1992). Consequently, the steady state ion concentration ('space charge') between a specimen and the ring electrode is strongly sample dependent. In the absence of cascade amplification (i.e. under conditions of low field strength whereby gas molecules are only ionized by primary and backscattered electrons), suppression of the SE signal by a space charge was noted by Farley & Shah (1990). It has recently been shown that, under typical low vacuum SEM operating conditions (i.e. whereby SEs are accelerated to energies sufficiently high to ionize gas molecules), the electric field generated by positive ions can significantly perturb the accelerating field generated by V and, consequently, alter contrast in SE images (Toth & Phillips, 2000a,b). In this paper we demonstrate the effects of SE–ion recombination on the number of electrons admitted to the gas cascade and consequent effects on image contrast. If the SE–ion recombination rate is inhomogeneous across a sample surface, lateral variations in the recombination rate can govern SE contrast, cause edge-darkening and, consequently, give rise to reversal of contrast exhibited by topographic features in images obtained using the current induced in a biased electrode (e.g. ESD and GSED images).

Based on theoretical arguments, existing models of SE cascade amplification were developed under the assumption that the effects of SE–ion recombination are negligible (Danilatos, 1990; Thiel *et al.*, 1997; Toth & Phillips, 2000a). Durkin & Shah (1993) have invoked the idea of electron–ion recombination in order to account for differences between calculated and measured gas amplification profiles of imaging signals in a low vacuum SEM. However, their theoretical approach seems inadequate in the light of subsequent work on processes occurring in the gas cascade (Fletcher *et al.*, 1997; Thiel *et al.*, 1997). The experimental results presented here suggest that, under normal low vacuum SEM operating conditions, SE–ion recombination can suppress a significant fraction of emitted SEs. Accordingly, this SE signal suppression mechanism should be accounted for in models of cascade amplification in low vacuum SEMs.

Background theory

In this section we provide a brief overview of the theory of electron–ion recombination in the context of signal formation in low vacuum SEMs and a discussion of the effects of applied electric fields on lateral inhomogeneities in the ion flux at the sample surface. For clarity, it is desirable to distinguish between recombination of ions with (i) thermalized electrons in the sample (low energy electrons, at or below the Fermi level as shown in Fig. 2, in thermal equilibrium with the lattice), (ii) hot electrons excited in the sample by the electron beam (energetic electrons residing in states above the Fermi level, as shown in Fig. 4(a)), and (iii) free electrons (emitted SEs and BSEs located above the sample surface).

(i) Thermalized electron–ion recombination

Accounts of experimental and theoretical investigations into recombination between positive gas ions and thermalized electrons can be found in reviews on ion neutralization spectroscopy (Hagstrum, 1978) and slow particle induced electron emission (Varga & Winter, 1992). A number of possible adiabatic recombination paths are illustrated schematically in the electron energy diagrams shown in Fig. 2. A metal surface is represented by the Fermi level (ε_{fermi}, the electrochemical potential of electrons in the metal) and the vacuum level (ε_{vac}, the energy of an electron at rest, in vacuum, infinitely far from the surface) (Kittel, 1986). The attractive ionic potential is in the form of a well which, as the metal–ion separation decreases, lowers the potential barrier that an electron at the surface must surmount to be captured in a stationary ionic state. Vacant ionic states are represented by open circles, occupied surface states by filled circles. In resonance neutralization

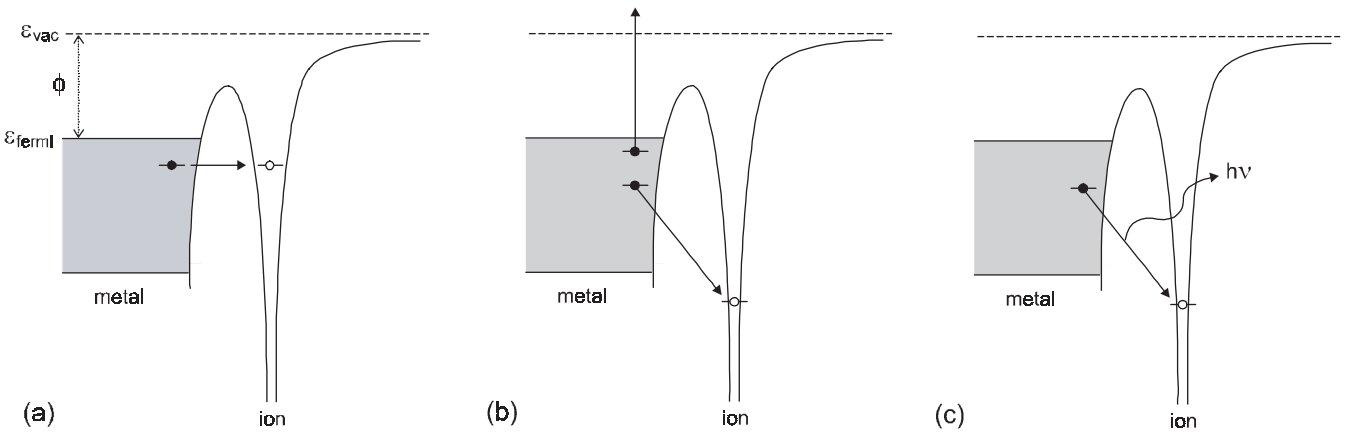

Fig. 2. Schematic illustrations of a number of thermalized electron–ion recombination paths: (a) resonance neutralization, (b) Auger neutralization, and (c) radiative neutralization (adapted from Hagstrum, 1978). [ε_{vac} = vacuum level, ε_{fermi} = Fermi level, ϕ = work function].

(Fig. 2(a)), an electron is transferred from the sample surface to an excited state of an ionized gas molecule that is energetically degenerate with the surface state. Auger neutralization (Fig. 2(b)) and radiative neutralization (Fig. 2(c)) involve the transfer of an electron from the surface to a more tightly bound state. Energy is conserved by the emission of an Auger electron or a photon. For singly charged ions the former is more probable because the Auger transition lifetime is about 10^6 times shorter than the radiative lifetime of approximately 10^{-8} s.

The transition rates of the above recombination processes are related to the overlap of surface state and ionic wave functions. Electrons captured by ions therefore originate almost exclusively from the first monolayer of the sample. As such, the thermalized electron–ion recombination rates are determined by the density of occupied electronic surface states, the height of the surface barrier, the ionic species and charge state, and the surface–ion separation.

The extent of overlap between the wave function of a surface state and an adjacent ionic state decreases with increasing binding energy of valence electrons in the solid. Consequently, insulators are expected to exhibit lower thermalized electron–ion recombination rates than metals, consistent with differences in the steady state ion concentration (space charge density) observed in a low vacuum SEM specimen chamber during SE imaging of conductors and insulators (Toth & Phillips, 2000a,b). It therefore follows that the SE imaging signals and the rate of space charge dissipation in variable pressure SEMs are sensitive to sample properties that affect the surface barrier. For example, the presence of water films on the sample surface and, in the case of insulators, metallic coatings and subsurface charge modify (i) the SE yield, (ii) the energy spectrum of emitted SEs (and hence, as discussed below, the SE–ion recombination rate), (iii) the thermalized and hot electron–ion recombination rates, and (iv) the space charge density (which in turn perturbs the detector field, the SE cascade amplification efficiency and the ion generation rate).

In the case of a grounded conductor imaged in a variable pressure SEM, the removal of electrons from the sample through electron–ion recombination gives rise to electron flow from ground to the specimen (i.e. the sample is maintained at ground potential). The total specimen current, often termed the 'ion current' and used as an imaging signal in low vacuum SEMs (Danilatos, 1990; Farley & Shah, 1990, 1991; Mohan *et al.*, 1998), is also contributed to by (i) current flow induced by the motion of charge carriers (electrons and ions) in the specimen chamber (Danilatos, 1990; Durkin & Shah, 1993; Mohan *et al.*, 1998; Toth & Phillips, 2000b) and (ii) the 'conventional' specimen current measured in high vacuum SEMs (i.e. the beam current less the emissive SE and BSE currents (Newbury, 1976)).

(ii) Hot and free electron–ion recombination

Energy distributions of hot electrons ($N_0(\varepsilon)$) excited in a metal by primary and backscattered electrons, and of emitted SEs (free electrons, $N_{SE}(\varepsilon)$) (Bindi *et al.*, 1980; Rösler & Brauer, 1981, 1991) are illustrated schematically in Fig. 3. Detailed discussions of known free electron–ion recombination processes can be found in the review by Hahn (1997) and references therein. In the context of electron imaging in low vacuum SEMs, the most relevant property of SE–ion recombination is the dependence of the recombination processes on SE energy. In the energy range of interest (< 50 eV), due to the Coulombic nature of the free electron capture process, the efficiency with which ions recombine with free electrons generally rapidly decreases with increasing electron energy (Hahn, 1997). Hence, SE–ion recombination is expected to preferentially suppress the low energy component of the SE signal. It has been suggested that such preferential recombination is responsible for anomalies in the pressure dependence of SE contrast caused by localized charging of insulators (Toth *et al.*, 2000). A detailed discussion of the effects of positive ions, localized sample charging and applied electric fields on SE

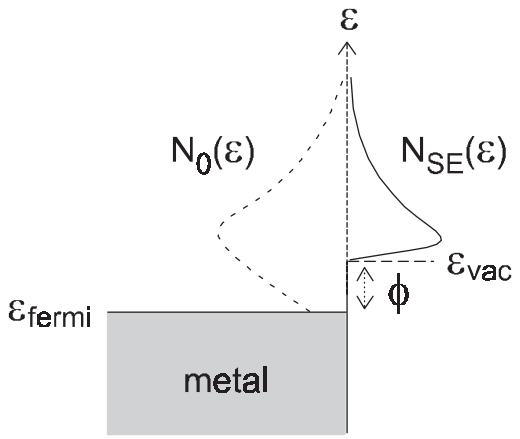

Fig. 3. Schematic illustration of energy distributions of SEs excited in a metal by primary and backscattered electrons (hot electrons, $N_0(\varepsilon)$) and of emitted SEs (free electrons, $N_{SE}(\varepsilon)$). [ε_{vac} = vacuum level, ε_{fermi} = Fermi level, ϕ = work function].

emission from insulators in variable pressure SEM chambers will be presented in a forthcoming publication. The following discussion will be restricted to the case of conductors.

Hot electrons generated in a metal by primary and backscattered electrons (see Fig. 3) can, based on their energy, be captured by positive ions through tunnel and free electron capture processes. Hot electrons with energies below the vacuum level (ε_{vac}) can recombine via the processes illustrated in Figs 2 and 4(b). Conversely, electrons with energies greater than ε_{vac} can recombine via the above mentioned free electron–ion recombination mechanisms. Hence, both the specimen and SE emission currents are affected by hot electron–ion recombination.

(iii) Ion flux distribution at the sample surface

If a sample located below the biased ring electrode in a low pressure SEM (see Fig. 1) contains topographic asperities, electric field lines generated by V preferentially terminate on the asperities, as is schematically illustrated in Fig. 5. Provided that the ionic mean free path is sufficiently long and the field generated by V is sufficiently intense, the instantaneous directions of the ion velocity vectors are approximately equal to the local electric field direction. In this case, most ions come into contact with the sample at points where the field line concentration maximizes. That is, the ion flux (which affects the steady state ion concentration) and, consequently, the electron–ion recombination rate are not uniform across the sample surface, but are enhanced in regions where the electric field line concentration maximizes. Hence, under conditions of long ionic mean free path and high field strength, the presence of topographic asperities (see Fig. 5) serves to make the spatial dependence of the electron–ion recombination rate across the sample surface inhomogeneous.

SE–ion recombination can, in principle, occur at high enough rates to decrease significantly the number of SEs that are amplified in the gas cascade and to suppress the signal used to form GSED images (Toth *et al.*, 2000). As SEs are accelerated by the field generated by V and can rapidly attain energies in excess of 100 eV (Thiel *et al.*, 1997), such recombination is only expected to be significant near the sample surface. Laterally, the recombination rate should scale with the ion flux. Hence, as an electron beam is rastered over a region that contains topographic asperities, the SE–ion recombination rate is a function of beam position. Such changes in the SE–ion recombination rate during image acquisition affect the number of SEs admitted to the gas cascade, modulate the intensity of the imaging signal induced in the ring electrode and can, in principle, produce contrast in images.

Experimental

Images presented in this paper were obtained using a GSED installed on an ElectroScan model E3 environmental scanning electron microscope (FEI Company, Peabody, MI) (ESEM) operated using an accelerating voltage of 20 kV (i.e. the images were generated using current measured from the biased ring electrode schematically illustrated in Fig. 1). The ion current was measured using a Keithley model 427 current amplifier (Keithley, Cleveland, OH). Backscattered electron images were obtained using an Everhart–Thornley detector (Reimer, 1985)

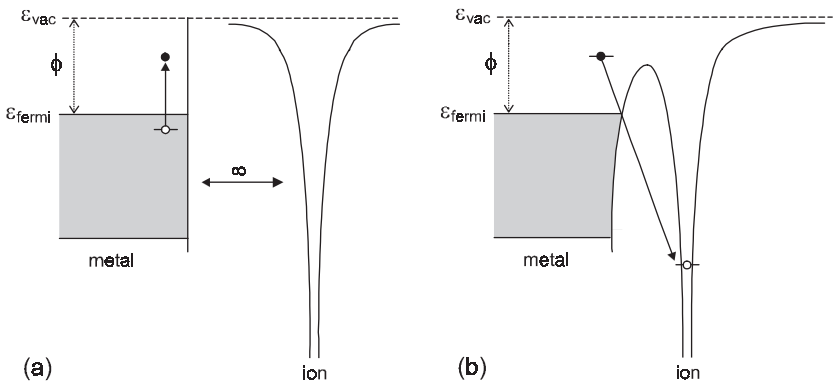

Fig. 4. Schematic illustrations of (a) a hot electron (filled circle) excited in a metal by an electron beam and the potential of an ion infinitely far from the metal surface, and (b) hot electron-ion recombination (where energy can be conserved via radiative, Auger and non-radiative processes). [ε_{vac} = vacuum level, ε_{fermi} = Fermi level, ϕ = work function].

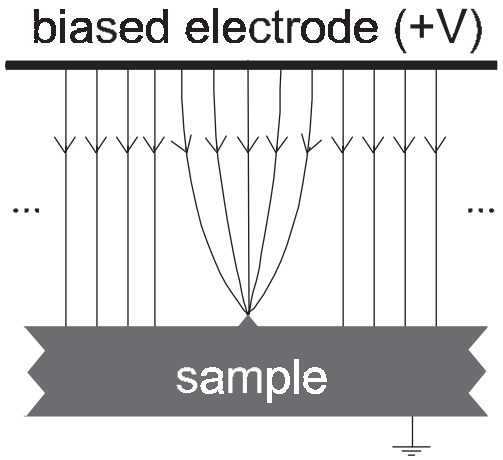

Fig. 5. Schematic diagram of a specimen–positively biased electrode system illustrating the effects of a topographic asperity on the local electric field line distribution. The field intensity, inversely proportional to field line separation, maximizes in the vicinity of such asperities.

(operated in passive mode with zero bias on the scintillator) installed on an FEI Philips XL30 FEG ESEM.

Results and discussion

Figure 6 shows GSED images of electrically grounded Al foil. The sample consists of three layers marked on Fig. 6(a): #1 – a top-most layer of Al with a relatively blunt edge (e_1); #2 – a centre layer of the same material, with an abrupt edge (e_2); #3 – an underlayer of Al with a surface texture different from the two overlayers. Electric field lines generated between the sample and the ring electrode by the ring bias, V, are expected to preferentially terminate at the two edges, particularly the abrupt edge, e_2. Such preferential termination of electric field lines on topographic asperities is schematically illustrated in Fig. 5. The intensity of the field generated by V should therefore maximize in the vicinity of e_2.

Validity of the proposed effects of SE–ion recombination on the GSED signal can be tested by acquiring GSED images as a function of parameters that affect how inhomogeneous the local ion concentration is across the sample surface (i.e. the extent to which ion trajectories are affected by the field line distribution). Figure 6 shows GSED images of Al foil acquired at pressures of 3, 2.5 and 1 Torr (0.40, 0.33, 0.13 kPa, respectively). At 3 Torr, the edge e_2 marked on Fig. 6(a) exhibits edge-brightening, as expected from conventional theory of electron emission (Reimer, 1985). As the pressure was decreased, the intensity of the GSED signal from e_2 decreased to the point where the edge appeared dark with respect to the rest of the sample (see Figs 6(b) and (c)). It should be noted that such edge-darkening can not be accounted for by (i) the effects of topography on electron emission (abrupt edges exhibit enhanced, not reduced electron emission (Reimer, 1985)), (ii) charging (as the sample is a grounded conductor), nor (iii) any

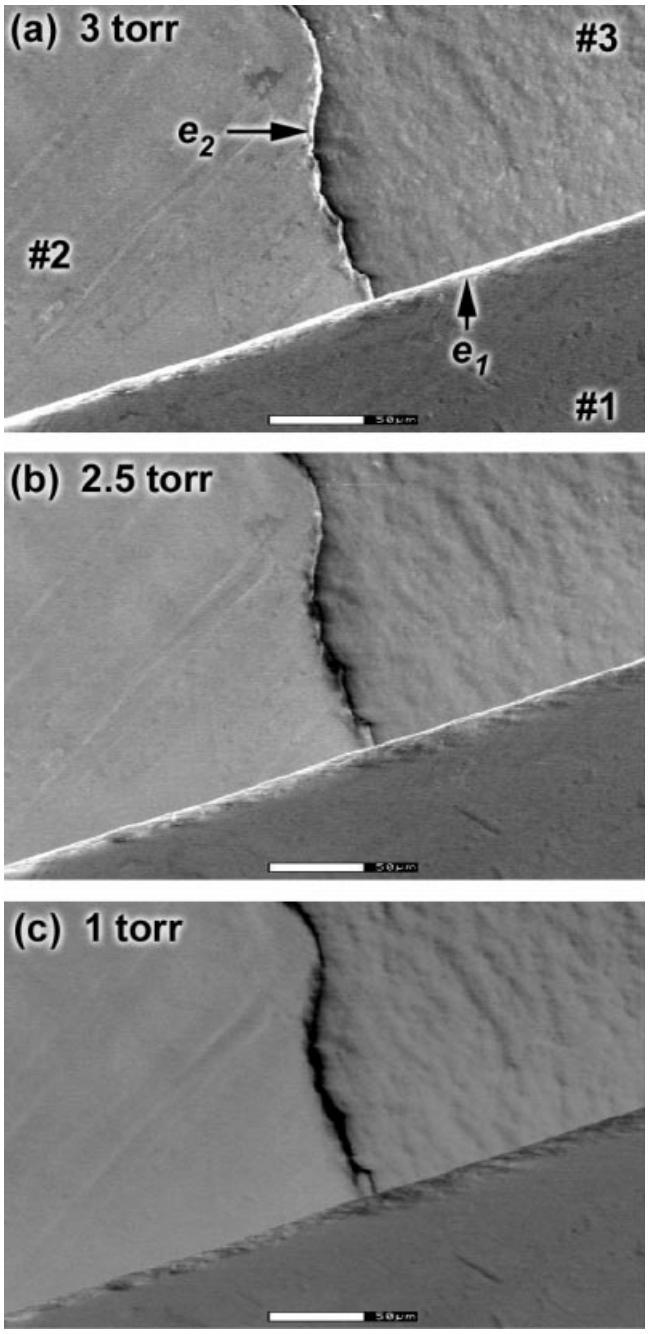

Fig. 6. GSED images of three layers of grounded Al foil acquired as a function of pressure: #1 – a top-most layer of Al with a relatively blunt edge (e_1); #2 – a centre layer of the same material, with an abrupt edge (e_2); #3 – an underlayer of Al with a surface texture different from the two overlayers. Contrast from edge e_2 inverted as the pressure was decreased from 3 to 1 Torr (0.39–0.13 kPa) (i.e. edge-darkening was observed under conditions of low pressure and high field strength). [gas = H_2O, V = 460 V, d = 1.7 mm].

effects caused by the pressure dependence of image contrast arising from variations in sample-ring electrode separation across the imaged region of the specimen, i.e. path length of emitted electrons in the imaging gas (as the relative intensities

of the GSED signal from flat regions of the 3 layers of Al shown in the figure did not change with pressure, i.e. the top-most layer (#1) appears darkest at all pressures). The edge-darkening also cannot be accounted for by charge flow induced (in the ring electrode) by rapid variations in the concentration of positive ions under the ring (Toth & Phillips, 2000b). The latter was only observed at high scan rates and under conditions of low field strength (corresponding to low ring electrode biases, V). The edge-darkening effect reported here was only observed under conditions of high field strength and the presence of inverted contrast was not dependent on scan rate.

The observed contrast inversion is, however, consistent with the above-mentioned effects of SE–ion recombination on the SE component of the imaging signal. In the gas cascade, ions are generated between the sample and the ring electrode. The generation rate minimizes at the sample surface, and maximizes in the vicinity of the ring (Thiel *et al.*, 1997). Ions produced in the gap between the sample and the ring drift towards the specimen under the influence of the electric field generated by V. At relatively high pressures (Fig. 6(a)), the ion trajectories are randomized by elastic collisions with gas molecules. Laterally, the ion flux is therefore homogeneous across the sample surface irrespective of the electric field line distribution. As such, in the vicinity of the surface, the electron–ion recombination rate is spatially homogeneous, the SE–ion recombination rate is independent of beam position and SE contrast is governed by variations in the SE yield (Fig. 6(a)). As the pressure is decreased, the ion–gas molecule collision frequency decreases (i.e. the ionic mean free path increases) and the correlation between the instantaneous direction of the ion velocity vectors and the direction of the local electric field increases. That is, under conditions of high field strength and low pressure, ion trajectories are parallel to the field lines and, near the sample surface, the ion flux (and hence the electron–ion recombination rate) maximizes at topographic asperities (see Fig. 5). In the case of the Al foil shown in Fig. 6, the steady state ion concentration maximizes at e_2. During image acquisition, when a scanning beam is incident on flat regions of the sample, SEs are amplified in the cascade in the usual manner, and most ions recombine with thermalized electrons (located in the vicinity of the first monolayer of the surface) at e_2. When the beam is incident on e_2, emitted SEs are available for recombination with ions above the sample surface (through the above-mentioned free electron–ion recombination mechanisms). The greater the SE–ion recombination rate, the smaller the number of SEs that enter the cascade, and the lower the magnitude of the imaging signal induced in the ring electrode (i.e. the GSED signal). Edge darkening is expected to occur under conditions whereby such beam-position-dependent modulation of the imaging signal by lateral variations in the SE–ion recombination rate is greater than the 'normal' changes in signal intensity caused by variations in the yields of SEs and BSEs that do not recombine with ions and enter the gas cascade (Fig. 6(c)).

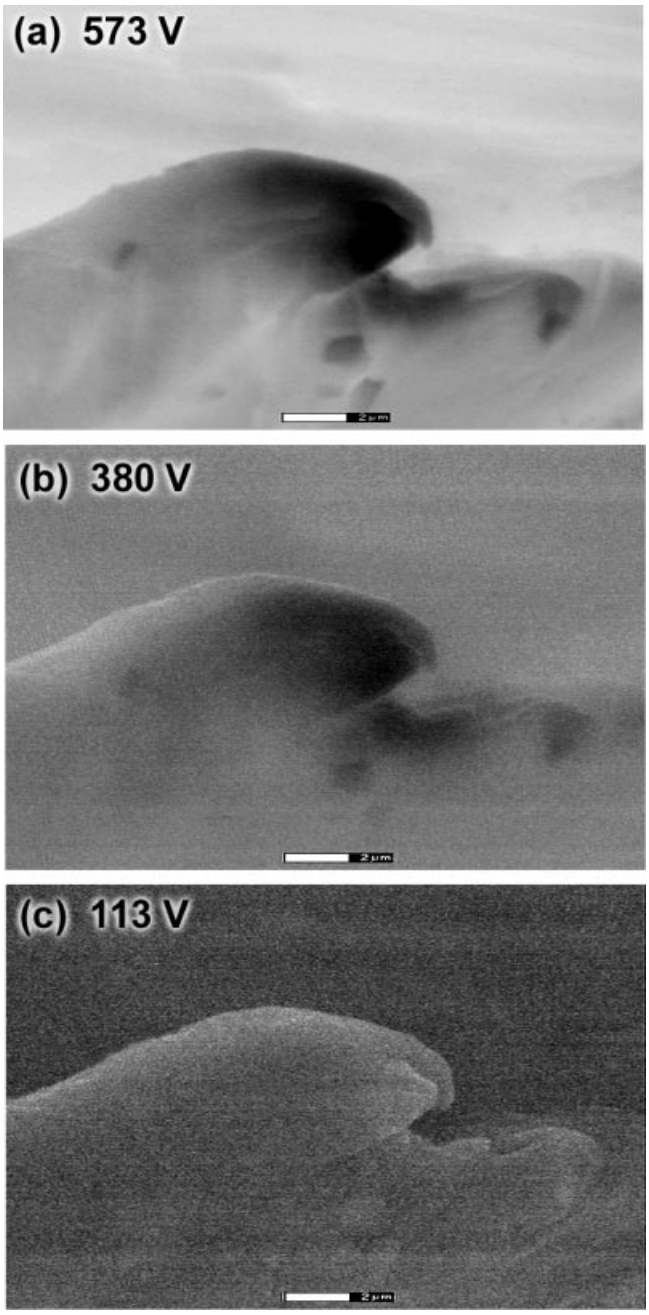

Fig. 7. GSED images of a grounded Al disk acquired as a function of V. Under conditions of high field strength (high V), some topographic features exhibit inverted contrast. [gas = H_2O, P = 0.4 Torr (0.05 kPa), d = 2.5 mm].

We note that whenever the imaging signal is suppressed by an increase in the SE–ion recombination rate, the ion flux is reduced, as fewer electrons enter the gas cascade and ionize gas molecules. However, the ion flux is never completely quenched because, even in the absence of SE cascade amplification, ions are produced by cascade amplification of primary and backscattered electrons (Moncrieff *et al.*, 1978).

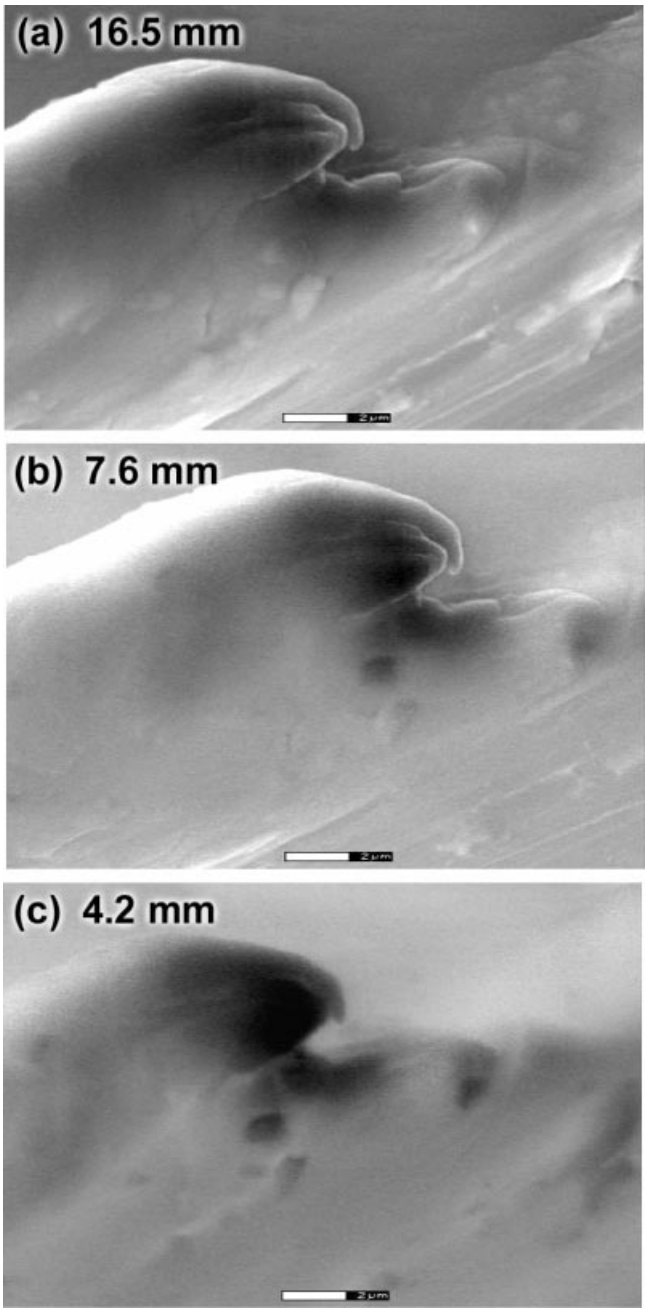

Fig. 8. GSED images of a grounded Al disk acquired as a function of sample-ring electrode separation (d). Under conditions of high field strength (short *d*), some topographic features exhibit inverted contrast. [gas = H_2O, $P = 0.4$ Torr (0.05 kPa), $V = 573$ V].

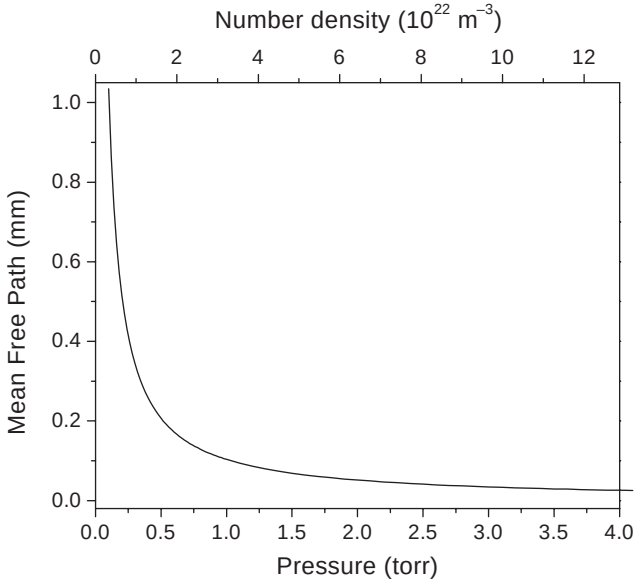

Fig. 9. Mean free path of H_2O molecules in water vapour calculated as a function of pressure.

The extent to which the instantaneous directions of the ion velocity vectors are affected by the direction of the local electric field is also a function of the field strength. The higher the field strength, the faster the response of an ion travelling with a given momentum to local changes in the direction of the electric field vector. That is, the higher the field strength, the greater the correlation between ion trajectories and the field line geometry, and the greater the extent to which the ion flux maximizes in the vicinity of topographic asperities. Figures 7 and 8 show GSED images of a rough, grounded Al disk acquired as a function of *V* and sample–detector separation, respectively. In both cases, inverted topographic contrast was only observed under conditions of high field strength (i.e. under conditions of high *V* and short sample-electrode separation). Inverse topographic contrast restored back to normal if the field strength was decreased by either decreasing *V* or increasing *d* (see Figs 7 and 8), as expected from the proposed SE–ion recombination contrast formation mechanism. The same contrast behaviour was observed in images of the abrupt edge e_2 of the Al foil shown in Fig. 6 that were acquired as a function of *V* and *d*.

The above interpretation of edge darkening is based on the assumption that, under conditions of 'low' pressure and 'high' field strength, the ionic mean free path is of the order of *d*. This assumption can be tested simply by calculating (i) the pressure dependence of the mean free path of neutral H_2O molecules in water vapour and (ii) the effects of applied electric fields on the kinetic energy of singly charged ions. The mean free path of a gas molecule (λ) in its parent gas can be approximated by (Present, 1958):

$$\lambda = (\sqrt{2\pi n\sigma})^{-1} \quad (1)$$

where *n* is the number density of gas molecules and σ is the collision cross-section (in the hard sphere approximation, the H_2O radius ~2.76 Å (Eisenberg & Kauzmann, 1969)). The decrease in λ_{water} with increasing pressure is shown in Fig. 9. For example, as *P* is decreased from 1 to 0.1 Torr, λ_{water} increases from approximately 0.1–1 mm (it should be noted that σ for most gases does not vary significantly; however,

Table 1. Kinetic energy (ΔKE) gained by a singly charged positive ion due to the action of an electric field ($|\vec{E}| = V/d$) over a distance equivalent to the mean free path ($\lambda(P)$) of a neutral H_2O molecule in water vapour.

		ΔKE (eV)		
P (Torr)	λ (μm)	$\|E\|$ = 50 kV m^{-1}	$\|E\|$ = 100 kV m^{-1}	$\|E\|$ = 250 kV m^{-1}
0.1	1035	52	103	259
0.2	517	26	52	129
0.5	207	10	21	52
1	103	5	10	26
2	52	2.6	5.2	13
5	21	1.0	2.1	5.2
10	10	0.5	1.0	2.6

subtle effects such as a decrease in λ at a given pressure are expected for heavier gases).

The electric field ($|\vec{E}| = V/d$) generated by V serves to increase the kinetic energy and mean free path of ionized gas molecules (von Engel, 1965; Nasser, 1971). To a first approximation, the gain in kinetic energy (ΔKE) can be calculated by assuming that λ_{water} is the distance traversed by an ion between elastic ion–H_2O scattering events. Table 1 shows λ_{water} and ΔKE calculated at a number of pressures between 0.1 and 10 Torr (0.013–1.3 kPa), and field strengths of 50, 100 and 250 kV m^{-1}. The calculated ΔKE values lie in the range 0.5–259 eV (the thermal energy of gas molecules at room temperature is 0.025 eV). The calculations provide an indication of the pressure dependence of the field strength required to change the kinetic energy of a singly ionized molecule by a given amount. For example, a gain of 2.6 eV requires field strengths of 50 and 250 kV m^{-1} at pressures of 2 and 10 Torr (0.27 and 1.3 kPa), respectively.

The calculated values of λ_{water} and ΔKE (Fig. 9 and Table 1) show that, at pressures below approximately 1 Torr (0.13 kPa) and under electrode biases of several hundred volts, the ionic mean free path can be in excess of several hundred micrometres. Combined with the fact that the ion–gas molecule forward scattering probability increases with collision energy (von Engel, 1965; Nasser, 1971), the above calculations illustrate that the lateral ion flux distribution at the sample surface can be affected by the geometry of the electric field generated by V.

The contrast reversal effect discussed in this paper was not observed in BSE images, consistent with the strong energy dependence of electron–ion recombination efficiencies reported in the literature. The fact that the BSE–ion recombination rate is negligible is also reflected in differences between the behaviour of contrast observed in images acquired using the GSED and the environmental secondary detector (ESD). The ESD signal contains a greater BSE component than the GSED signal (Fletcher *et al.*, 1999). Consequently, edge-darkening in ESD images was observed over a narrower range of operating parameters than in corresponding GSED images (i.e. lower pressures and greater field strengths were required to produce contrast inversion in ESD images).

Contrast reversal was observed in images obtained using the large field GSED, a gaseous electron detector in which the ring electrode shown in Fig. 1 is replaced by a biased metal plate located off-axis, near the pole piece, above the sample surface (FEI, 2000). However, the inverted contrast persisted over a different range of operating parameters from that observed using the GSED and ESD, probably due to differences in the sample-detector-pole piece geometry (and corresponding differences in the detector field strength and field line distribution).

Edge contrast reversal was also not observed in images generated using the ion current (see Fig. 1). This can be understood in the light of differences between the signal components that make up the net signals induced in the ring and stage electrodes. SE–ion recombination suppresses the rate at which SEs enter the cascade and, consequently, lowers: (i) the rate at which ion–electron pairs are generated in the cascade, (ii) the flux of electrons and ions moving through the gas, and (ii) the currents induced in the ring (i.e. ESD and GSED signals) and stage (i.e. ion current signal) electrodes. This reduction in cascade amplification and in the ion current gives rise to an inverted contrast component in both the net ion current and GSED signals. However, unlike the GSED signal, the ion current contains additional components that give rise to 'normal' contrast under all operating conditions: (i) as in the case of the ESD (Fletcher *et al.*, 1999), the specimen current contains a greater BSE component (which is never inverted) than the GSED signal, and (ii) the emission of electrons (SEs and BSEs) from the sample contributes to 'normal' contrast in ion current images irrespective of whether the SEs recombine with ions, or enter the cascade. Hence, a greater number of processes contribute to the 'normal contrast' component of the net ion current signal than of the biased ring electrode signal. In principle, an inverted contrast component is expected to be present in the ion current signal, but it was not observed to dominate over the 'normal contrast' components under any operating conditions.

From a practical viewpoint the contrast reversal effects discussed in this paper can be identified by acquiring images as a function of parameters that affect the field strength (e.g. detector bias and working distance) and ionic mean free path (e.g.

pressure). At present, it would be misleading to define regions of parameter space within which recombination contrast is present in SE images due to the strong dependence on the field geometry. The field line distribution is affected by sample morphology, shape and size, and the specimen stage-sample-detector-pole piece geometry, none of which are standardized in low vacuum SEMs. Furthermore, as will be discussed elsewhere, subsurface charging of insulators can significantly alter the detector field and introduce recombination contrast sensitivity to parameters such as beam current and scan speed, which do not affect recombination contrast in SE images of conductors. A device designed to control (and possibly standardize) the field line distribution, the effects of ions on cascade amplification and hence allow for meaningful specification of variable pressure SEM operating parameters will be described in an accompanying paper by Craven *et al.* (2002).

Finally, it should be pointed out that the magnitude of the SE–ion recombination rate observed when the ion flux is concentrated on specific regions of a sample implies that this SE suppression mechanism may also be significant under normal low vacuum operating conditions, despite the absence of inverted topographic contrast in images generated using the current induced in a biased electrode. When normal contrast is observed in SE images produced using the ring electrode imaging signal, the ion flux is approximately constant over the specimen surface and electron–ion recombination does not give rise to contrast in SE images. However, laterally homogeneous recombination uniformly suppresses the SE component of the ring electrode signal and affects the pressure dependence of gas gain amplification (as the magnitude of gas gain and hence the ion generation and SE–ion recombination rates are dependent on pressure). Incorporation of the effects of recombination into the theory of gas gain amplification may account for discrepancies between calculated and measured gas gain behaviour (Fletcher *et al.*, 1997; Thiel *et al.*, 1997). Furthermore, if the ion flux is homogeneous across the imaged region of a specimen, the SE–ion recombination rate must scale with the area from which SEs are emitted. That is, at high beam energies ($E_b > \approx 5$ keV), type II SEs (secondary electrons generated by backscattered electrons (Reimer, 1985)) should recombine with ions more efficiently than type I SEs (secondary electrons generated by primary electrons (Reimer, 1985)). Such signal filtering may be beneficial if the high resolution of the type I SE signal is desirable (at the expense of the higher signal-to-noise ratio exhibited by the type II SE signal).

Conclusion

The results presented here provide experimental evidence for the effects of electron–ion recombination on SE contrast in images obtained using low vacuum SEMs. Under conditions of low pressure and high electric field strength (i.e. high electrode bias and short sample–electrode separation), SE–ion recombination can cause edge-darkening in images generated using the current induced in a biased electrode (e.g. the ESD and GSED signals). Consequently, under such conditions, contrast formed by variations in the magnitude of SE signal suppression caused by electron–ion recombination can dominate the net imaging signal, and topographic asperities can exhibit inverted contrast. Contrary to assumptions made in existing models of the behaviour of partially ionized gases in low vacuum SEM chambers, the presented results demonstrate that electron–ion recombination causes significant SE signal suppression and, as such, must be accounted for in theories of signal behaviour and image formation.

Acknowledgements

We gratefully acknowledge stimulating discussions with John Craven, Frank Baker, Debbie Stokes, Matthew Phillips, David Joy and Archie Howie. This work was funded by EPSRC and FEI corporation.

References

Bindi, R., Lanteri, H. & Rostaing, P. (1980) A new approach and resolution method of the Boltzmann equation applied to secondary electron emission, by reflection from polycrystalline aluminium. *J. Phys. D*, **13**, 267–280.

Craven, J.P., Baker, F.S., Thiel, B.L. & Donald, A.M. (2002) Consequences of positive ions on imaging in low vacuum SEM. *J. Microsc.* **205**, 96–105.

Danilatos, G.D. (1988) Foundations of environmental scanning electron microscopy. *Adv. Electronics Electron Phys.* **71**, 109–250.

Danilatos, G.D. (1990) Theory of the gaseous detector device in the environmental scanning electron microscope. *Adv. Electronics Electron Phys.* **78**, 1–102.

Durkin, R. & Shah, J.S. (1993) Amplification and noise in high-pressure scanning electron microscopy. *J. Microsc.* **169**, 33–51.

Eisenberg, D. & Kauzmann, W. (1969) *The Structure and Properties of Water*. Clarendon Press, Oxford.

von Engel, A. (1965) *Ionized Gases*. Clarendon Press, Oxford.

Farley, A.N. & Shah, J.S. (1990) Primary considerations for image enhancement in high-pressure scanning electron microscopy. *J. Microsc.* **158**, 389–401.

Farley, A.N. & Shah, J.S. (1991) High-pressure scanning electron microscopy of insulating materials: a new approach. *J. Microsc.* **164**, 107–126.

FEI (2000) *Xl30 ESEM FEG SEM Operating Instructions*. FEI Company, Boston.

Fletcher, A.L., Thiel, B.L. & Donald, A.M. (1997) Amplification measurements of alternative gases in environmental SEM. *J. Phys. D*, **30**, 2249–2257.

Fletcher, A.L., Thiel, B.L. & Donald, A.M. (1999) Signal components in the environmental scanning electron microscope. *J. Microsc.* **196**, 26–34.

Hagstrum, H.D. (1978) Studies of adsorbate electronic structure using ion neutralization and photoemission spectroscopies. *Electron and Ion Spectroscopy of Solids* (ed. by L. Fiermans, J. Vennik & W. Dekeyser), pp. 273–323. Plenum Press, New York.

Hahn, Y. (1997) Electron-ion recombination processes – an overview. *Report Prog. Phys.* **60**, 691–759.

Kittel, C. (1986) *Introduction to Solid State Physics*. John Wiley & Sons, New York.

Meredith, P., Donald, A.M. & Thiel, B.L. (1996) Electron–gas interactions in the environmental scanning electron microscope's gaseous detector. *Scanning*, **18**, 467–473.

Mohan, A., Khanna, N., Hwu, J. & Joy, D.C. (1998) Secondary electron imaging in the variable pressure scanning electron microscope. *Scanning*, **20**, 436–441.

Moncrieff, D.A., Robinson, V.N.E. & Harris, L.B. (1978) Charge neutralisation of insulating surfaces in the SEM by gas ionisation. *J. Phys. D*, **11**, 2315–2325.

Nasser, E. (1971) *Fundamentals of Gaseous Ionization and Plasma Electronics*. Wiley-Interscience, New York.

Newbury, D.E. (1976) The utility of specimen current imaging in the SEM. *Scanning Electron Microscopy*, **1**, 111–120.

Present, R.D. (1958) *Kinetic Theory of Gases*. McGraw-Hill, New York.

Reimer, L. (1985) *Scanning Electron Microscopy*. Springer, Berlin.

Robinson, V.N.E. (1975a) The elimination of charging artefacts in the scanning electron microscope. *J. Phys. E*, **8**, 638–640.

Robinson, V.N.E. (1975b) Wet stage modification to a scanning electron microscope. *J. Microsc*. **103**, 71–77.

Robinson, V.N.E. (1978) The SEM examination of wet specimens. *Scanning*, **1**, 149–156.

Rösler, M. & Brauer, W. (1981) Theory of secondary electron emission. *Phys. Stat. Sol. B*, **104**, 161–175, 575–587.

Rösler, M. & Brauer, W. (1991) Theory of electron emission from nearly-free-electron metals by proton and electron bombardment. *Particle Induced Electron Emission I*. Springer-Verlag, Berlin, pp. 1–65.

Stokes, D.J., Thiel, B.L. & Donald, A.M. (1998) Direct observations of water-oil emulsion systems in the liquid state by environmental scanning electron microscopy. *Langmuir*, **14**, 4402–4408.

Thiel, B.L., Bache, I.C., Fletcher, A.L., Meredith, P. & Donald, A.M. (1997) An improved model for gaseous amplification in the environmental SEM. *J. Microsc*. **187**, 143–157.

Toth, M., Kucheyev, S.O., Williams, J.S., Jagadish, C., Phillips, M.R. & Li, G. (2000) Imaging charge trap distributions in GaN using environmental scanning electron microscopy. *Appl. Phys. Lett*. **77**, 1342–1344.

Toth, M. & Phillips, M.R. (2000a) The effects of space charge on contrast in images obtained using the environmental scanning electron microscope. *Scanning*, **22**, 313–319.

Toth, M. & Phillips, M.R. (2000b) The role of induced contrast in images obtained using the environmental scanning electron microscope. *Scanning*, **22**, 370–379.

Varga, P. & Winter, H. (1992) Slow particle-induced electron emission from solid surfaces. *Particle Induced Electron Emission II*. Springer-Verlag, Berlin, pp. 149–214.